Title: Grain-size properties and organic-carbon stock of Yedoma Ice Complex permafrost from the Kolyma lowland, northeastern Siberia

Jens Strauss[1], Lutz Schirrmeister[1], Sebastian Wetterich[1], Andreas Borchers[1], and Sergei P. Davydov[2]

[1]Alfred Wegener Institute for Polar and Marine Research, Periglacial Research Unit Potsdam, Telegrafenberg A43, 14473 Potsdam, Germany

[2]Northeast Scientific Station, Pacific Institute for Geography, Far-East Branch, Russian Academy of Sciences, Republic of Sakha, Yakutia, 2 Malinovy Yar St., 678830 Cherskii, Russia.

Author List:

Jens Strauss, Jens.Strauss@awi.de, Alfred Wegener Institute for Polar and Marine Research, Periglacial Research Unit Potsdam, Telegrafenberg A43, 14473 Potsdam, Germany

Lutz Schirrmeister, Lutz.Schirrmeister@awi.de, Alfred Wegener Institute for Polar and Marine Research, Periglacial Research Unit Potsdam, Telegrafenberg A43, 14473 Potsdam, Germany

Sebastian Wetterich, Sebastian.Wetterich@awi.de, Alfred Wegener Institute for Polar and Marine Research, Periglacial Research Unit Potsdam, Telegrafenberg A43, 14473 Potsdam, Germany

Andreas Borchers, Andreas-Bo@nexgo.de, Alfred Wegener Institute for Polar and Marine Research, Periglacial Research Unit Potsdam, Telegrafenberg A43, 14473 Potsdam, Germany

Sergei Davydov, davydoffs@mail.ru, Northeast Scientific Station, Pacific Institute for Geography, Far-East Branch, Russian Academy of Sciences, Republic of Sakha, Yakutia, 678830 Cherskii, Russia

Abstract

The organic carbon stock in permafrost is of increasing interest in environmental research, because during the late Quaternary a large pool of organic carbon accumulated in the sedimentary deposits of arctic permafrost. Because of its potential to degrade and release organic carbon, the organic-matter inventory of Yedoma Ice Complex deposits is relevant to current concerns about the effects of global warming. In this context, it is essential to improve the understanding of preserved carbon quantities and characteristics. The paper aims to clarify the Yedoma Ice Complex origin, and to develop an approach for volumetric organic-matter quantification. Therefore, we analyzed the grain size and the organic-matter characteristics of the deposits exposed at the stratigraphic key site Duvanny Yar (lower Kolyma River, northeast Siberia). A distinct bimodal grain-size distribution confirms a polygenetic origin of the frozen sediments from a flood-plain environment. The total organic-carbon content averages 1.5 ± 1.4 wt% while the volumetric organic-carbon content averages 14 ± 8 kg/m³. However, large-scale extrapolations for Yedoma Ice Complex deposits in general are not reasonable yet because of their rather unclear spatial distribution. We conclude that Yedoma Ice Complex formation at Duvanny Yar was dominated by water-related (alluvial/fluvial/lacustrine) as well as aeolian processes. The total organic-carbon content of the studied deposits is low if compared to other profiles, but it is still a significant pool.

1. Introduction

A large pool of organic carbon accumulated in arctic permafrost during the late Quaternary, representing a significant long-term carbon sink. According to recent estimations, about half of the global below-ground organic carbon is stored in permafrost soils (1024 Gt in the first three meters depth below surface) [*Tarnocai et al.*, 2009]. In addition to the upper permafrost soil layers and peatlands [e.g. *Hugelius and Kuhry*, 2009], the fine-grained late

Pleistocene Yedoma Ice Complex (IC) deposits are believed to contain a huge organic-carbon inventory [*Zimov et al.*, 2006a]. Yedoma IC deposits are well-exposed along the coasts and riverbanks in the northern East Siberian lowlands. *Kanevskiy et al.* [2011] and *Schirrmeister et al.* [2011a] give a detailed definition of a Yedoma IC deposits; they describe it as remnant hills of a former surface plain, which rises by several dozens of meters above the surrounding terrain.

Polar regions respond more quickly and more strongly to climate change than do other regions on Earth [e.g. *Rigor et al.*, 2000; *Johannessen et al.*, 2004; *Graversen et al.*, 2008]. With regard to climate change, it is predicted that Yedoma ICs will be transformed from carbon reservoirs to carbon sources if these organic-rich sediments thaw and greenhouse gases are subsequently released [*Walter et al.*, 2006; *Zimov et al.*, 2006a; *Schuur et al.*, 2008; *Kuhry et al.*, 2009]. Recent attention has focused on the fossil organic matter in such deposits [e.g. *Schirrmeister et al.,* 2011b], although detailed studies of the size of the carbon pool, the level of release risk, and the release timescales are still rare. This study focuses on the Yedoma IC deposition environment to achieve a better understanding of sediment properties and organic-carbon stock, and employs the sedimentary archive of two Yedoma IC profiles at the Duvanny Yar permafrost section, located at the right lower Kolyma riverbank. The samples were taken during the joint Russian-German Beringia/Kolyma 2008 expedition [*Wetterich et al.*, 2011.] The objectives of this paper are (1) to deduce the origin of the Duvanny Yar Yedoma IC deposits from its grain-size properties, and (2) to develop a new volume-based approach for quantifying organic carbon in permafrost.

2. Material and Methods

2.1 Study site

Duvanny Yar is considered to be a stratigraphic key site for the late Quaternary [*Kaplina et al.*, 1978; *Sher et al.*, 1979] and an important reference site for the late Pleistocene history

of Beringia [*Hopkins*, 1982]. Beringia is the former interconnected landmass stretching from the Taymyr Peninsula to Alaska which was not glaciated during the late Quaternary. Duvanny Yar (68° 37'N, 159° 06'E, **Fig. 1**) is situated on the right bank of the lower Kolyma River in the northeastern part of Yakutia. *Lopatina and Zanina* [2006] and *Zanina et al.* [2011] describe the study site location and its research history in detail.

The Duvanny Yar section was first described by *Barandova* [1957] and *Biske* [1957]. *Sher* [1971] studied horse bones paleozoologically and differentiated the permafrost sequence in a lower mid Pleistocene and an upper late Pleistocene part. Cryolithological and sedimentological structures of Duvanny Yar were described in detail by *Kaplina et al.* [1978], *Arkhangelov et al.* [1979], *Sher et al.* [1979], and *Konishchev* [1983]. *Vasil'chuk et al.* [1988] worked on stable isotope data and pollen records from ice wedges. Paleopedological studies were carried out by *Gubin* [1995]. *Vasil'chuk et al.* [2001] suggested that the Duvanny Yar Yedoma IC deposits accumulated between ~40 and 13 ka BP. More recent studies are about soil respiration and methane production [*Dutta et al.* 2006; *Zimov et al.* 2006a].

The Yedoma IC deposits are exposed in an approximately 12-km-long outcrop, which consists of Yedoma hills as high as 50 m above river level (a.r.l.) dissected by deep thermo-erosional valleys and thermokarst depressions. *Giterman et al.* [1982] differentiate the Duvanny Yar section stratigraphically into four units. At river level, unit I is described as last interglacial lacustrine silts in ice-wedge pseudomorphs. Unit II is composed of woody and peaty sediments from the mid Pleistocene. Unit III is described as the late Pleistocene Yedoma IC which is investigated in this study (**Fig. 2**). The uppermost unit IV is the Holocene cover on top of the Yedoma IC.

Based on field observations, a general description of the matrix and color, cryostructures, and organic compounds of the various paleocryosol and homogeneously-composed deposits of the geological sections is given in the results section.

2.2 Field work

The Yedoma IC profiles were studied and sampled in sub-profiles exposed on separate thermokarst mounds (baydzherakhs) in river cliff thaw slumps. After cleaning the sample profiles, the exposed deposits were described according to sediment characteristics and cryostructures, photographed, and sketched. To consider a maximized sediment sequence, various sub-profiles from different thermokarst mounds were stacked together into a composite profile. To determine the absolute ice content (ice content in relation to wet sample weight), frozen samples were placed in aluminum boxes and weighed. Boxed samples were dried on an oven and then weighed again to calculate the absolute ice content using the weight difference.

2.3 Grain-size distribution

The grain-size distribution (GSD) between 0.375 and 1000 µm was analyzed using a laser particle sizer (Beckmann-Coulter LS 200). In order to measure only clastic grains and to disaggregate the sample, organic components were removed by adding 35 % hydrogen peroxide three times a week to the samples which were shaken for 6 weeks. The organic-free samples were diluted and 'washed' to neutral pH values by centrifugation. After that, the samples were dispersed in 1 % ammonia solution and 1 g dispersing agent ($Na_4P_2O_7 \cdot 10\ H_2O$) and shaken for 5 hours. Finally, the samples were repeatedly split and two sub-samples were analyzed and averaged. The resulting GSD comprises 92 grain-size classes. GSD results were used in the calculation of grain-size parameters (mean diameter, sorting and skewness) used for the lithostratigraphical classification. Grain-size parameters were calculated after *Folk and Ward* [1957] using the Gradistat software [*Blott and Pye*, 2001]

2.3.1 End-member modeling

Statistical analysis of the GSD curves was performed using an end-member (EM) modeling algorithm written with Matlab software by *Dietze et al.* [2011]. Compared to other statistical procedures, EM modeling provides a statistically and genetically meaningful solution by unmixing compositional data sets [*Weltje,* 1997; *Weltje and Prins*, 2007].

Important criteria for obtaining feasible models include insuring that EMs are non-negative, and that they fulfill the constant-sum constraints. EMs are defined by two characteristics: first the loadings, which are the GSDs of the EMs, and second the scores, which typify their quantitative variation throughout the profile. In this study, grain-size data were transformed using a W-transformation after *Manson and Imbrie* [1964] and *Klovan and Imbrie* [1971] as described in *Miesch* [1976] and *Weltje* [1997]. To minimize effects of scale, this transformation of the data is necessary [*Dietze et al.,* 2011].

2.3.2 Interactive peak fitting

Interactive peak fitting (IPF, Version 4.1) [*O'Haver*, 2009] was the second method used to segregate the components of compositional data sets and to separate changes in the processes of sediment transportation and accumulation. Unlike EM modeling, IPF needs minor mathematical presumptions for GSD peak decomposition. Like EM modeling, IPF partitioning reveals information about the transport and deposition processes affecting each component. The IPF software is a Matlab extension for time-series signals and uses an unconstrained nonlinear optimization algorithm to separate an overlapping peak signal. The peak type was set to Gaussian distribution. The Gaussian normal function is often used to describe the statistical law of polymodal GSDs [e.g. *Ashley*, 1978]. Fitting experiments by *Sun et al.* [2002] indicate that the normal function also works on samples with asymmetrical components. Every GSD was fitted graphically by applying it to several Gaussian curves (**Fig. 3**) until the root mean square (RMS) error was acceptable (< 2). Finally, the percentage of each mode area compared to the total curve area was calculated. The area of the Gaussian curves is taken because it provides a more robust estimate than other measured parameters like position, height, and width.

2.4 Biogeochemistry

Total organic carbon (TOC) and total nitrogen (TN) contents and TOC/TN (C/N) ratios reflect variations in bioproductivity, organic matter accumulation, composition, and degradation [*Meyers*, 1994]. Before measurement, the samples were homogenized and milled using a planetary mill. Therefore, coarser organic fragments are also included in the TOC content. For very organic-rich samples, sinter-corundum instead of agate grinding jars were used. Carbonate was removed by hydrochloric acid (4 % HCl). Samples were then wrapped in tin foil. The sediment samples were measured twice with a carbon-nitrogen-sulfur (CNS) analyzer (Elementar Vario EL III). In each series of measurements a blank capsule was used for background detection and standards were measured after every 20 samples to ensure correct analytical values with a device-specific accuracy of ± 0.1 wt%. For the TN measurements the procedure was the same, except different calibration standards and no carbonate removal procedures were used.

The carbon isotope content (δ^{13}C) of TOC was measured with a Thermo Finnigan MAT Delta-S mass spectrometer. Measuring control standards at the beginning of each run and repeating control measurements after every seventh experimental measurement ensured correct analytical values of better than ± 0.15 ‰ compared against the Vienna Pee Dee Belemnite (VPDB) standard.

Bulk density is a pedological standard parameter describing the mass of a volume unit of soil. The total volume includes both solid and pore volume. In this study, the bulk density of the sediment was determined to be the basic parameter for volumetric carbon quantification to account for ice-rich permafrost deposits. The density of the solid fraction (ρ_s, 10^3kg/m³) was measured using a helium gas displacement pycnometer (AccuPyc-1330, Micromeritics). For bulk density (ρ_b, 10^3kg/m³) calculation the volume of the solids (V_s, 10^{-6}m³). Moreover, the mass of solid particles (m_s) is used in equation 1.

$$V_s = \frac{m_s}{\rho_s} \tag{1}$$

was derived first. After that, the porosity (n)

$$n = \frac{V_p}{V_p + V_s} \tag{2}$$

was calculated using the volume of the pores (V_p, 10^{-6}m³). Finally, determining the negative linear correlation

$$\rho_b = (n-1) \cdot (-\rho_s) \tag{3}$$

[*Horn*, 2002] with the sediment porosity allows bulk density to be calculated.

For most parts of Yedoma IC it is convenient to assume that all pores are ice-saturated. We defined ice content >20 wt% as threshold for ice saturation. With this assumption, the absolute ice content gives an estimation of the pore volume. For the determination of ice volume ($V_{ice} = m_{ice}/\rho_{ice}$) an ice density of 0.91 10^3kg/m³ [*Lide et al.*, 2008] was assumed.

For calculating the organic-carbon inventory, the density measurements were combined with TOC values. The reference volume (V_{ref}) was chosen to be 1 m³. The volumetric organic carbon (C_{org}) calculation (kg TOC /m³) was performed according to:

$$\text{volumetric } C_{org} \text{ content} = V_{ref} \cdot \rho_b \cdot \frac{TOC_{wt\%}}{100}. \tag{4}$$

3. Results

3.1 Lithological features of the Yedoma Ice Complex

The results refer to a lower profile, DY-05, and an upper profile, DY-01 (**Fig. 2**). The two profiles were not stacked together because there was a distance of approximately two kilometers between them [*Wetterich et al.*, 2011]. The Yedoma IC sequence was subdivided into 2 groups, consisting of paleocryosols 1 to 5 (**Fig. 2** and **Fig. 4**) and more homogeneously-composed sediments.

We use the term paleocryosol to designate buried or fossil frozen soils horizon, which were found at various heights within the Yedoma IC deposits. These horizons differ from the surrounding sediment by the presence of brownish and dark-brown patches, indicating enrichment by plant and wood fragments, and higher TOC contents as well as cryoturbation features.

In the lower paleocryosol sequence (**Fig. 4**, 1.3 to 6.8 m a.r.l., including paleocryosols 1 to 3) of profile DY-05, the deposits contain plant detritus, dark-brown patches, and wood fragments such as shrub twigs or roots. The matrix of light-brown fine sand contains numerous filamentous roots and black spots. The cryostructures are banded, laminated-lenticular, or micro-lenticular. In some places, horizontal ice bands 2 to 3 cm thick as well as separate ca. 3-cm-long vertical ice veins occur. Here, the absolute ice content reaches 65 wt%. A distinct 5-cm-thick peaty horizon, paleocryosol 4, occurs at 10.8 m a.r.l. This former soil horizon is distinguished by dark-brown peat inclusions up to 2-3 cm in diameter, cryoturbation, filamentous roots, single plant remains, and horizontal micro to fine lens-like cryostructures and a high ice content (42 wt%). The dark-brown paleocryosol 5 with organic bands, cryoturbation, and peaty organic and larger wood fragments (**Fig. 4**) occurs between 28.8 and 29.1 m a.r.l. in profile DY-01. Here, the cryostructures are irregular lenticular with diagonal ice veins and ice segregation around wood fragments. Like in the paleocryosols 1 to 4 below, high ice content (53 wt%) of this paleocryosol covaries with high TOC content (10.5 wt%).

The homogeneous part of the Yedoma IC also contains roots, plant fragments, and peat materials, and hence supported vegetation during exposed conditions. Unlike paleocryosols 1 to 5, no clear evidence for pedogenesis is visible. The homogeneous parts of the Yedoma IC at DY-05 consist of light grey-brown sandy silt with filamentous roots. The cryostructure is structureless (no visible ice) to micro-lenticular and the absolute ice content varies up to 41

wt%. Some separate parts contain larger, more distributed plant fragments and peat inclusions.

3.2 Granulometric characteristics and calculations

Grain-size analysis of the DY-05 and DY-01 profiles reveals a homogeneous composition (**Fig. 5a, b**). All samples are poorly to very-poorly sorted (mean sorting degree after *Folk and Ward* [1957] 2.1 ± 0.1) clayish to sandy silts (mean grain-size diameter 9 to 24 µm, mean skewness 0.3). The GSD curves show a distinct bimodal distribution with a smaller peak in the fine-silt fraction (between 3 and 4 µm) and a larger peak between 40 and 60 µm. A less-distinct third peak in the fine-sand fraction is found in some samples, which is most pronounced at 16, 22, and 23 m a.r.l. The mentioned differentiation of the paleocryosol at 28.8 to 29.1 m a.r.l. (paleocryosol 5) is shown in the sand fraction as well. Here, the lowest sand content occurs and the GSD curve stands out from the general pattern, because of a relative enrichment in the medium-silt fraction.

3.2.1 End-member modeling

The mean coefficient of determination (R² mean) displays the explained variance of each modeled grain-size class. It was calculated to estimate the minimum number of EMs required to adequately represent the original data. *Weltje* [1997] and *Prins and Weltje* [1999] showed that the minimum adequate number of EMs corresponds to the position of the inflection point of the 'number of end-members - explained cumulative variance' curve (0.88 for 2 EMs, **Fig. 6a,** grey curve). For the Yedoma IC sediments of Duvanny Yar, the R^2 indicates that two EMs (**Fig. 6a, black curve**) are adequate to describe the original grain-size dataset. The model with two EMs explains 55 % of the total variance (R² mean 0.55, **Fig 6a and d**). **Fig. 6c** shows that the modeling error is independent of the profile height. The R² statistics of the single grain-size classes (**Fig. 6d**) reveal that the highest uncertainties are found in the coarse (> 100 µm) size classes and at the point of intersection of the two EMs. The uncertainty of the

coarse fraction is caused by low absolute content of material within this size class, and thus relatively high modeling errors compared to classes with greater amounts of material. The low R^2 at the point of intersection (**Fig. 6d**) is the result of a modeling error induced by the simplification to two EMs. To improve the R^2, especially at the intersection point, it is possible to increase the number of EMs (Fig. 6a). However, following the law of parsimony we decided to use only 2 EMs. For the studied deposits more EMs are difficult to interpret in a sedimentological context and the risk of over-interpreting our data would rise precipitously.

EM 2 is characterized by an approximately unimodal GSD with a maximum in the fine-to-medium-silt fraction (**Fig. 6b**). In the paleocryosol sequence, including paleocryosols 1 to 3, EM 2 scatters across a wide range, from 6 to 100 % (**Fig. 7**). The range in the homogeneously-composed deposits of DY-05 is smaller, with a mean value of 60 %. Paleocryosol 5 shows scores of up to 100 % for EM 2. Here, the GSDs are characterized by two peaks of nearly the same size and height. Above, the mean value of EM 2 stabilizes, as it did in the homogeneously-composed deposits of DY-05, at around 67 %. EM 1 is characterized by a unimodal GSD with a maximum at the coarse silt - fine sand border (~62 µm). Because of the constant-sum constraint the development of EM 1 is opposite to that of EM 2.

3.2.2 Interactive peak fitting grain size pattern

Like the EMs, the IPF-separated peaks were attributed to the supposed main mechanisms of transportation and sedimentation.

In the application of IPF the areas of Gaussian curves 5 and 4 as well as 3 and 2 (**Fig. 3a**) were merged (**Fig. 3a**) due to the assumption that each Gaussian pair, 5+4 and 3+2, are related to the same processes. This assumption is evident by the linear relationship of the pairs (**Fig. 3b, c**). In profile DY-05, the area of peak 5+4 ranges between 29 and 54 % (median 41 %) and in profile DY-01 between 32 and 57 % (median 44 %). In profile DY-05, peak 3+2 ranges between 43 and 69 % (median 58 %). With some exceptions, this grain-size peak is the

major one and therefore represents the main sedimentation process. Like in the lower Yedoma IC profile, peak 3+2 at DY-01 is the largest with an area between 37 and 68 % (median 53 %), but a smaller gap between the median of peak 5+4 and peak 3+2 reveals a diminishing influence of peak 3+2.

The value of the minor peak 1 in the fine-sand fraction is between <1 and 6 %. In some samples this peak is not clearly obvious.

3.2.3 Assumptions for end-member modeling and interactive peak fitting interpretation

For grain-size modeling with EMs and 'graphical' fitting with IPF, the different GSDs are attributed to the supposed main mechanisms of transportation and sedimentation. Both methods (EM and IPF) have been applied in sedimentology [e.g. *Sun et al.,* 2002; *Dietze et al.*, 2011] and possibly support each other. The main mechanisms are chosen on the basis of natural EMs, like loess deposits from Alaska (Schirrmeister, unpublished data) and from China [*Sun et al.*, 2002] as well as floodplain deposits from China [*Kaakinen and Lunkka*, 2003; *Kenkkilä*, 2005] (**Fig. 6**). The supposed main mechanisms causing the GSDs are water related (alluvial/fluvial/lacustrine) processes (including loess reworked by water). Floodplain overbank deposition is assumed for EM 2 and peak 5+4, and aeolian for EM 1 and peak 3+2. The small peak 1 is termed fluvial/aeolian because its GSD allows no clear distinction to be made. After *Sun et al.* [2002] this small peak as well as the small peak of EM 2 and the shoulder of EM 1 can be interpreted as a signal of the saltation component of alluvial/fluvial/lacustrine and aeolian processes.

3.3 Organic matter characteristics and calculations

The C/N ratio indicates the degree of organic-matter decomposition due to microbial activities and pedogenic processes (low ratios: more strongly decomposed; high ratios: less decomposed [*Kumada*, 1987; *Ping et al.*, 1998]). Furthermore, paleoclimatic information is stored in organic-carbon data. Variations in $\delta^{13}C$ values indicate different origins of organic

matter (e.g. marine, terrestrial, sub-aerial/aquatic), and the degree of decomposition of plant material by different processes of isotopic fractionation during carbon turnover. Lower $\delta^{13}C$ values indicate less-decomposed organic matter, while higher $\delta^{13}C$ indicate that stronger decomposition has occurred [*Meyers*, 1994]. The TOC values and C/N ratio in paleocryosols 1 to 5 (**Fig 4**) are variable. High TOC values of >4 wt% and C/N ratios of >12 occur. C/N ratios of up to 15 reveal a small degree of organic-matter decomposition compared to the homogeneous Yedoma IC (C/N ~8). The TOC content in the homogenously-composed Yedoma IC remains constant, between 1 and 2 wt%, in the majority of the samples. A deviation from the homogenous pattern is observed for the low C/N ratio (4.5) at 20.5 m a.r.l., where the ice content is higher.

The $\delta^{13}C$ in the paleocryosols ranges from -27.4 to -25.6 ‰. This is lighter than the homogeneous parts, which range from -25.9 to -24.6 ‰. The $\delta^{13}C$ value of the permafrost deposits can be interpreted as an integrative signal of e.g. seasonal effects, water conditions [*Welker et al.*, 1993; *Gundelwein et al.*, 2007], and decomposition rates [*Pfeiffer and Jansen*, 1993].

The estimated bulk density was combined with the TOC contents to calculate the volumetric organic-carbon content (**Eq. 4**). Bulk density of the homogeneous sequences primarily varied due to ice content rather than to TOC content because the latter was relatively low (< 2 wt%). The lower paleocryosol sequence (1.3 to 6.8 m a.r.l.) is characterized by a bulk density that alternates between 0.4 and 1.2 10^3 kg/m³. The organic-carbon content spans a wide range, between 6 and 37 kg/m³. The mean value of 19 kg/m³ at the paleocryosol sequence is significantly higher than in the homogenous Yedoma IC units. Paleocryosol 4 contains 31 kg/m³. Paleocryosol 5 with its peat inclusions and high ice content exhibits a minimum bulk density and maximum volumetric organic-carbon content (63 kg/m³). Over the entire range of the homogeneously-composed deposits, the volumetric organic-carbon content was below 20 kg/m³ (mean 12 kg/m³). The total mean volumetric

organic-carbon content of the Yedoma IC deposits at Duvanny Yar is 14 ± 8 kg/m³. For the active layer of Kolyma Lowland soils, *Mergelov and Targulian* [2011] report an average volumetric organic-carbon stock of 15.1 kg C/m^2, with the greater part of organic carbon (60–90%) in the mineral part of the soils. In our calculation we exclude the active layer and the Holocene cover on top of the Yedoma IC. Our calculated organic-carbon stock provides evidence that the deeper mineral horizons contain nearly as much carbon as the active layer, emphasizing the great significance of the deep fossil organic carbon pool.

4. Discussion

4.1 Origin of the Yedoma Ice Complex at Duvanny Yar

The studied Kolyma River cliff cut in vertically- or diagonally-polygonal ice-wedge systems. It is suggested that the Yedoma hills are remnants of former accumulation plains [e.g. *Schirrmeister et al.,* 2011a]. There is still no widely accepted concept of Yedoma ICs genesis, but it seems clear that neither glacial-related sedimentation, such as hypothesized by *Nagaoka et al.* [1995] and *Grosswald* [1998], nor shallow-marine sedimentation, such as postulated by *Bol'shiyanov et al.* [2009], was involved. An overview of the different Yedoma ICs origin concepts is given by *Vasil'chuk* [1992].

It is agreed that Yedoma IC material was sub-aerially exposed most of the time and froze syngenetically during permafrost accumulation [*Kanevskiy et al.*, 2011]. Based on more than 50 radiocarbon dates for adjacent sediments [*Vasil'chuk et al.*, 2001], we know that the ice wedges at Duvanny Yar were formed between ~37 and 13 ka BP by syngenetic freezing of permafrost deposits. Our studies confirm the syngenetic freezing process because lenticular and layered cryostructures occur. The average absolute ice content of all studied deposits is 35 wt%. Assuming that ice wedges can account for about 50 vol% in Yedoma IC sequences [*Schirrmeister et al.*, 2002; *Zimov et al.*, 2006a], the total absolute ground-ice content can constitute up to three quarters of the total outcrop volume. This clearly shows the

vulnerability of Yedoma IC deposits to warming temperatures and surface subsidence during thawing.

Three granulometric characteristics can be seen in the GSDs (**Fig. 5**). First, a sand maximum, as shown by the sand maximum sample at 6.1 m a.r.l., could be caused by a higher energetic transport level such as increased streaming velocity during a flooding period, as has been suggested by our EM modeling. In some samples a distinct third small peak in the fine-sand fraction is obvious. This can be explained by an increased fraction of seasonal or temporal inundation of a floodplain due to stronger streaming conditions or increased aeolian activity resulting in enrichment of the fine-sand fraction by a larger fraction of saltating and rolling sediments [*Reineck and Singh*, 1980]. Second, an enrichment of the finer fractions, especially the medium-silt fraction, like in paleocryosol 5, can indicate ponding water, in which the settling velocity of the suspended medium-silt fraction allows for its deposition [*Hjulström*, 1939]. At this paleocryosol our EM 2 for alluvial, fluvial, and lacustrine processes rises to 100 %. Additionally, the increased TOC could be caused by ponding water and boggy conditions in low-center polygons, under which the accumulation of organic matter is higher and the decomposition rate is lowered. Third, paleocryosols are characterized by more alternating mean grain sizes. This could be a consequence of faster environmental changes, increased plant growth, or thaw and cryoturbation processes during warmer periods. Despite these specific characteristics, the grain-size analysis and magnetic susceptibility data indicate stable sediment sources as well as persistent transport conditions.

Loess material, formed as a result of cryogenic weathering and glacial grinding processes, is rather common in (peri)glacial environments and drifts from outwash plains via aeolian transport. Therefore, *Pye* [1995] defined a sub-category of loess named 'periglacial loess'. Moreover, *Pye* [1987] states that the GSD of a 'typical' loess shows a pronounced mode in the 28 to 48 µm range and is positively skewed (towards the finer sizes). *Smalley and Smalley*

15

[1983] define loess-sized material as between 20 to 60 µm, which corresponds perfectly with the observed large peak of the studied deposits.

Sub-aquatic fluvial and lacustrine silts can also be loess-like, as can some alluvial and colluvial deposits [*Konishchev*, 1987]. Especially the first peak, described by EM 2 and peak 5+4, cannot be explained by pure aeolian processes. *Walger* [1962] states that products of each of the three basic transport and deposition mechanisms, namely suspension, saltation, and rolling, are represented in every single GSD. However, because of sediment variations and sampling uncertainties, polymodal GSDs are recorded. Due to the absence of visible layered structures, and considering Walger's hypothesis, IPF and EM modeling were conducted. The results of these modeling efforts clearly indicate that the GSD of each single sample is characterized by at least bimodal curves and consists of numerous single populations of monomodal GSDs, indicating the participation of various processes of transport and (re-)sedimentation during Yedoma IC formation in agreement with a polygenetic formation concept [*Sher*, 1995; *Sher et al.,* 2005]. In this context, EM 2 is believed to be an alluvial, fluvial, and lacustrine signal, and EM 1 is interpreted as an aeolian component. IPF peak 4+5 is interpreted as the water-dependent analogue to EM 2, peak 3+2 as aeolian, and peak 1 as the fluvial/aeolian component (**Fig. 6b and 7**).

This interpretation of the GSDs is based on natural EMs like Chinese [*Sun et al.,* 2002] and Alaskan loess (Schirrmeister, unpublished data), as well as on alluvial/fluvial/lacustrine deposits from northern China [*Kaakinen and Lunkka*, 2003; *Kenkkilä*, 2005]. Another EM for periglacial loess(-like) sediment was described by *Zech et al.* [2008] at the Tumara palaeosol sequence in northeast Siberia.

Both EM modeling and IPF reveal a relatively balanced proportion of the peaks/distributions interpreted as the alluvial/fluvial/lacustrine component (EM: 61 ± 21 %; IPF: 43 ± 6 %) and the aeolian component (EM: 39 ± 21 %; IPF: 55 ± 7 %).

The consistency of the EM modeling and the IPF scores indicates stable accumulation conditions. Another process for producing fine-grained sediments could be *in-situ* frost weathering of the material. After deposition, repeated freezing and thawing of ice/water-bearing sediments results in production of silt-sized particles [*Konishchev and Rogov*, 1993; *Wright et al.*, 1998; *Schwamborn et al.*, 2008]. When this process is significant, the post-depositional transformation conceals the primary transport and accumulation signal, distorting and complicating the interpretation. In addition, winnowing/eroding of the fine fraction by shallow overland flow caused by rain or thawing events could have altered the depositional GSDs [*Farenhorst and Bryan*, 1995].

Due to the (very) poorly-sorted polymodal sediments lacking in carbonates, and the absence of glaciers and ice sheets with their grinding processes [*Seppälä*, 2004] in northeast Siberian lowlands [*Velichko et al.*, 1997; *Hubberten et al.*, 2004; *Svendsen et al.*, 2004], the Yedoma IC at Duvanny Yar is interpreted to be of polygenetic origin. Water-related (like floodplain overbank deposition) and aeolian deposition were the controlling processes. It is also likely that seasonally-differentiated deposition occurs here. A possible scenario of seasonal deposition is flooding of alluvial areas after snowmelt and during periods of high river discharge (today around June, Kolymskoye Stream Discharge Station, ArcticRIMS). Aeolian deposition likely occurs in dryer seasons. During fall and winter, river discharge volume is extremely reduced. As a consequence, parts of the formerly submerged floodplain areas become susceptible to wind activity [e.g. *Muhs and Bettis*, 2003].

4.2 Changes in organic matter parameters

The TOC content of the homogenous parts of the studied Yedoma IC deposits is between 0.5 and 2.0 wt%, which is rather low compared to other Yedoma IC studies (~4 wt%, *Schirrmeister et al.,* 2011b). The paleocryosols are characterized by TOC values of up to 10.5 wt%. The mean organic-carbon value for the whole profile is 1.5 ± 1.4 wt%, and the δ^{13}C values range between -27.4 and -24.6 ‰. These parameters, in combination with high C/N

ratios, suggest that fresh water and sub-aerial terrestrial environments were the dominant sources of organic matter during Yedoma IC formation. In the paleocryosol samples a higher input of terrestrial plant associations is revealed. The local environmental conditions under which the paleocryosol sequences were formed are likely to have been more humid and favorable for plant growth. Hence, the formation period of the lowermost paleocryosol sequence fits well into the Middle Weichselian (50 to 30 ka BP) interstadial period [*Schirrmeister et al.*, 2002]. This hypothesis is based on the stratigraphical position, and on parameters such as high TOC contents, high C/N ratios, and low δ^{13}C values (**Fig. 4**). These are typical indications of interstadial periods with increased bioproductivity and moderate organic-matter decomposition under wet/moist conditions [e.g. *Wetterich et al.*, 2009; *Schirrmeister et al.*, 2011c]. Moreover, the alternating behavior observed in the paleocryosols can be explained, according to *Gundelwein et al.* [2007], as the result of a patchy environment such as a distinctive mosaic-like polygonal tundra with moist anaerobic (lower δ^{13}C) and dryer aerobic conditions (higher δ^{13}C). On the contrary, in the homogeneously-composed sediments of the Yedoma IC stadial periods were characterized by less variable, generally lower TOC contents and low C/N ratios (higher decomposition). Despite the low TOC values compared to other Yedoma IC studies, the Yedoma IC at Duvanny Yar contains a considerable organic-carbon inventory with a mean of 14 ± 8 kg/m³. Given that the Yedoma IC deposits accumulated at relatively fast rates and low temperatures, the organic matter had only a short time to decompose before it was incorporated into a permanently-frozen state. Therefore, Yedoma IC deposits are believed to contain a labile and vulnerable carbon-matter stock. Applying broad upscaling, *Zimov et al.* [2006b] estimated the organic-carbon reservoir in Siberian ICs to be ~500 Gt.

Our data from Duvanny Yar show lower TOC content and lower bulk densities; therefore, we hypothesize that the Yedoma IC carbon inventory is lower than estimated by *Zimov et al.* [2006b]. Large-scale extrapolations should be considered as preliminary because of great

uncertainties about the controlling factors, e.g. Yedoma IC distribution/area, thickness, and local heterogeneity. When considering the different studies of spatial variation of carbon-bearing Yedoma IC deposits [e.g. *Walter et al.*, 2006; *Zimov et al.*, 2006b; *Tarnocai et al.*, 2009], it becomes obvious that our knowledge about the quantities and qualities of this organic-matter pool is insufficient for extrapolating possible effects of a warming climate on the Yedoma IC organic-carbon stock. Nevertheless, as a large carbon inventory that is vulnerable to release, the Yedoma IC deposits contain an important carbon pool, which is relevant to current discussions about the effect of global climate warming.

5. Conclusions

The very poor sorting of sediments, bi- to polymodal grain-size distributions, a lack of carbonate, and the absence of historic ice sheets in the region show the Yedoma Ice Complex at Duvanny Yar to be of polygenetic origin, formed in the polygonally-patterned floodplain of the Kolyma River. Alluvial and fluvial processes on a former floodplain and aeolian deposition were the controlling processes. Seasonally-differentiated deposition probably occurred.

The carbon inventory of Duvanny Yar amounts to 14 ± 8 kg/m³ (organic-carbon concentration 1.5 ± 1.4 wt%). Thus, the Yedoma Ice Complex deposits contain a significant carbon inventory. Large-scale extrapolations of the organic-carbon inventory should be considered preliminary because of great uncertainties about the controlling factors such as Yedoma Ice Complex area, thickness, and local heterogeneity.

References

Arkhangelov, A. A., V. V. Popov, and A. V. L'yanos-Mas (1979), About permafrost-facial structure of the Yedoma horizon of Dyvanny Yar, Kolyma Lowland, in *Problems of Cryolithology*, pp. 145-156, Moscow University Press, Moscow.

Ashley, G. M. (1978), Interpretation of polymodal sediments, *The Journal of Geology, 86*(4), 411-421.

Barandova, Y. P. (1957), Geomorphological sketch of the eastern part of the Kolyma Lowland, in *Materials for Geology and Resources of Northeast USSR*, Magadan Publishing House, Magadan.

Biske, S. F. (1957), Quaternary deposits of the Kolyma Lowlands, in *Materials for Geology and Resources of Northeast USSR*, Magadan Publishing House, Magadan.

Blott, S. J., and K. Pye (2001), GRADISTAT: A grain size distribution and statistics package for the analysis of unconsolidated sediments, *Earth Surface Processes and Landforms, 26*(11), 1237-1248, doi: 10.1002/esp.261.

Bol'shiyanov, D. Y., M. N. Grigoriev, W. Schneider, A. S. Makarov, and E. A. Gusev (2009), Sea-level fluctuations, and Ice Complex formation on the Laptev Sea coast during the Late Pleistocene, in *System of the Laptev Sea and the Adjacent Arctic Seas*, edited by H. Kassens, A. P. Lisitzin, J. Thiede, Y. I. Pelyakova, L. A. Timokhov, and I. E. Frolov, pp. 349-356, Moscow University Press, Moscow.

Brown, J., O. J. Ferrians, J. A. Heginbottom, and E. S. Melnikov (1997), Circum-Arctic map of permafrost and ground-ice conditions, US Geological Survey in Cooperation with the Circum-Pacific Council for Energy and Mineral Resources., Washington, DC.

Dietze, E., K. Hartmann, B. Diekmann, J. Ijmker, F. Lehmkuhl, S. Opitz, G. Stauch, B. Wünnemann, and A. Borchers (2011), An end-member algorithm for deciphering modern detrital processes from lake sediments of Lake Donggi Cona, NE Tibetan Plateau, China, *Sedimentary Geology*, doi: 10.1016/j.sedgeo.2011.09.014, in press.

Dutta, K., E. A. G. Schuur, J. C. Neff, and S. A. Zimov (2006), Potential carbon release from permafrost soils of Northeastern Siberia, *Global Change Biology*, *12*(12), 2336-2351.

Ehlers, J., and P. L. Gibbard (2003), Extent and chronology of glaciations, *Quat. Sci. Rev.*, *22*(15-17), 1561-1568, doi:10.1016/S0277-3791(03)00130-6.

Farenhorst, A., and R. B. Bryan (1995), Particle size distribution of sediment transported by shallow flow, *CATENA, 25*(1-4), 47-62, doi: 10.1016/0341-8162(94)00041-c.

Folk, R. L., and W. C. Ward (1957), Brazos River bar: A study in the significance of grain size parameters, *Journal of Sedimentary Petrology, 27*(1), 3-26.

Giterman, R. E., A. V. Sher, and J. V. Matthews (1982), Comparison of the development of tundra-steppe environments in west and east Beringia: Pollen and macrofossil evidence from key sections, in *Paleoecology of Beringia*, edited by D. M. Hopkins, J. V. Matthews, C. E. Schweger and S. B. Young, pp. 43-73, Academic Press, New York.

Graversen, R. G., T. Mauritsen, M. Tjernstrom, E. Kallen, and G. Svensson (2008), Vertical structure of recent Arctic warming, *Nature*, *451*(7174), 53-56, doi:10.1038/nature06502.

Grosswald, M. G. (1998), Late-Weichselian ice sheets in Arctic and Pacific Siberia, *Quat. Int.*, *45-46*, 3-18.

Gubin, S. V. (1995), Late Pleistocene soil formation on coastal lowlands of northern Yakutia, *Eurasian Soil Science*, *27*(5), 19-32.

Gundelwein, A., T. Müller-Lupp, M. Sommerkorn, E. T. K. Haupt, E. M. Pfeiffer, and H. Wiechmann (2007), Carbon in tundra soils in the Lake Labaz region of arctic Siberia, *Eur. J. Soil Sci.*, *58*(5), 1164-1174, doi:10.1111/j.1365-2389.2007.00908.x.

Hjulström, F. (1939), Transportation of detritus by moving water, in *Recent Marine Sediments: A Symposium*, edited by P. D. Trask, pp. 5-31, American Association of Petroleum Geologists, Tulsa.

Hopkins, D. M. (1982), Aspects of the paleogeography of Beringia during the Late Pleistocene, in *Paleoecology of Beringia*, edited by D. M. Hopkins, J. V. Matthews, C. E. Schweger, and S. B. Young, pp. 3-28, Academic Press, New York.

Horn, R. (2002), Bodenphysik, in *Scheffer/Schachtschabel - Lehrbuch der Bodenkunde*, edited by H.-P. Blume, G. W. Brummer, U. Schwertmann, R. Horn, I. Kögel-Knabner, K. Stahr, K. Auerswald, L. Beyer, A. Hartmann, N. Litz, A. Scheinost, H. Stanjek, G. Welp and B.-M. Wilke, pp. 155-271, Spektrum Akademischer Verlag, Heidelberg.

Hubberten, H.-W., A. Andreev, V. I. Astakhov, I. Demidov, J. A. Dowdeswell, M. Henriksen, C. Hjort, M. Houmark-Nielsen, M. Jakobsson, S. Kuzmina, E. Larsen, J. P. Lunkka, A. Lysa, J. Mangerud, P. Moller, M. Saarnisto, L. Schirrmeister, A. V. Sher, C. Siegert, M. J. Siegert, and J. I. Svendsen (2004), The periglacial climate and environment in northern Eurasia during the Last Glaciation, *Quat. Sci. Rev.*, *23*(11-13), 1333-1357, doi:10.1016/j.quascirev.2003.12.012.

Hugelius, G., and P. Kuhry (2009), Landscape partitioning and environmental gradient analyses of soil organic carbon in a permafrost environment, *Global Biogeochem. Cycles*, *23*(3), GB3006, doi:10.1029/2008gb003419.

Johannessen, O. M., L. Bengtsson, M. W. Miles, S. I. Kuzmina, V. A. Semenov, G. V. Alekseev, A. P. Nagurnyi, V. F. Zakharov, L. P. Bobylev, L. H. Pettersson, K. Hasselmann, and H. P. Cattle (2004), Arctic climate change: Observed and modeled temperature and sea-ice variability, *Tellus Ser. A*, *56*(4), 328-341, doi:10.1111/j.1600-0870.2004.00060.x.

Kaakinen, A., and J. P. Lunkka (2003), Sedimentation of the Late Miocene Bahe Formation and its implications for stable environments adjacent to Qinling mountains in Shaanxi, China, *Journal of Asian Earth Sciences, 22*(1), 67-78, doi: 10.1016/s1367-9120(03)00044-0.

Kanevskiy, M., Y. Shur, D. Fortier, M. T. Jorgenson, and E. Stephani (2011), Cryostratigraphy of late Pleistocene syngenetic permafrost (yedoma) in northern Alaska, Itkillik River exposure, *Quaternary Research*, *75*(3), 584-596, doi: 10.1016/j.yqres.2010.12.003.

Kaplina, T. N., R. E. Giterman, O. V. Lakhtina, B. A. Abrashov, S. V. Kiselyov, and A. V. Sher (1978), Duvannyy Yar - a key section of Upper Pleistocene deposits of the Kolyma lowland, *Bulletin of Quaternary Research Commission*, *48*, 49–65.

Kenkkilä, J. (2005), The laser diffraction grain size analysis of late Miocene flood-plain sediments from Lantian, in Shaanxi province, northern China, 43 pp, University of Helsinki.

Klovan, J., and J. Imbrie (1971), An algorithm and Fortran-IV program for large-scale Q-mode factor analysis and calculation of factor scores, *Mathematical Geology*, *3*(1), 61-77, doi: 10.1007/bf02047433.

Konishchev, V. N. (1983), Cryolithological evidences of the heterogeneous structure of "Ice Complex" deposits in the Dyvanny yar section, in *Problems of Cryolithology*, pp. 56-64, Moscow University Press, Moscow.

Konishchev, V. N. (1987), Origin of loess-like silt in Northern Jakutia, USSR, *GeoJournal*, *15*(2), 135-139, doi:10.1007/bf00157938.

Konishchev, V. N., and V. V. Rogov (1993), Investigations of cryogenic weathering in Europe and Northern Asia, *Permafrost Periglac.*, *4*(1), 49-64, doi:10.1002/ppp.3430040105.

Kuhry, P., C.-L. Ping, E. A. G. Schuur, C. Tarnocai, and S. Zimov (2009), Report from the International Permafrost Association: Carbon pools in permafrost regions, *Permafrost Periglac.*, *20*(2), 229-234, doi:10.1002/ppp.648.

Kumada, K. (1987), *Chemistry of Soil Organic Matter*, Elsevier/Japan Scientific Societies Press, Amsterdam.

Lide, D. R., G. Baysinger, H. V. Kehiaian, L. I. Berger, K. Kuchitsu, R. N. Goldberg, D. L. Roth, W. M. Haynes, and D. Zwillinger (2008), Properties of ice and supercooled water, in *CRC Handbook of Chemistry and Physics*, edited by D. R. Lide, G. Baysinger, H. V. Kehiaian, L. I. Berger, K. Kuchitsu, R. N. Goldberg, D. L. Roth, W. M. Haynes, and D. Zwillinger, p. 1101, CRC Press/Taylor and Francis, Boca Raton, Florida.

Lopatina, D., and O. Zanina (2006), Paleobotanical analysis of materials from fossil gopher burrows and upper Pleistocene host deposits, the Kolyma River lower reaches, *Stratigr. Geol. Correl.*, *14*(5), 549-560, doi:10.1134/s0869593806050078.

Manson, V., and J. Imbrie (1964), *FORTRAN Program for Factor and Vector Analysis of Geologic Data using an IBM 7090 or 7094/1401 Computer System*, 46 pp., Kansas Geol. Survey Spec. Distrib. Pub. 13, University of Kansas, Lawrence, Kansas.

Mergelov, N., and V. Targulian (2011), Accumulation of organic matter in the mineral layers of permafrost-affected soils of coastal lowlands in East Siberia, *Eurasian Soil Science,* *44*(3), 249-260, doi: 10.1134/s1064229311030069.

Meyer, H., K. Yoshikawa, L. Schirrmeister, and A. Andreev (2009), The Vault Creek Tunnel (Fairbanks region, Alaska): A Late Quaternary palaeoenvironmental permafrost record, in *Proceedings of the 9th International Conference on Permafrost*, edited by D. L. Kane and K. M. Hinkel, pp. 1191-1196, Institute of Northern Engineering - University of Alaska Fairbanks, Fairbanks

Meyers, P. A. (1994), Preservation of elemental and isotopic source identification of sedimentary organic matter, *Chem. Geol.*, *114*(3-4), 289-302, doi:10.1016/0009-2541(94)90059-0.

Miesch, A. T. (1976), Q-mode factor analysis of geochemical and petrologic data matrices with constant row sums, U.S. Geol. Survey Prof. Paper 574-G, 46 pp, U.S. Government Printing Office, Washington.

Muhs, D. R., and E. Bettis (2003), Quaternary loess-paleosol sequences as examples of climate-driven sedimentary extremes, in *Extreme Depositional Environments: Mega End Members in Geologic Time*, edited by M. A. Chan and A. W. Archer, pp. 53-74, *Geological Society of America Special Paper 370*, Boulder, Colorado.

Nagaoka, D., K. Saijo, and M. Fukuda (1995), Sedimentological environment of the edoma in high Arctic eastern Siberia, in *Proceedings of the Third Symposium on the Joint Siberian Permafrost Studies between Japan and Russia*, edited by K. Takahashi, A. Osawa, and Y. Kanazawa, pp. 8–13., Tsukuba, Japan.

O'Haver, T. C. (2009), *An Introduction to Signal Processing in Chemical Analysis*, 45 pp., University of Maryland, College Park, Maryland.

Péwé, T.L., 1975, *Quaternary geology of Alaska*, U.S. Geological Survey Professional Paper 835, 145 pp.

Pfeiffer, E. M., and H. Janssen (1993), Characterization of organic carbon, using the δ^{13}C-value of a permafrost site in the Kolyma-Indigirka-Lowland, northeast Siberia, in *Proceedings of the Meeting on the Classification, Correlation, and Management of Permafrost-Affected Soils, Alaska, USA*, edited by J. Kimble and R. J. Ahrens, pp. 90-98, USDA, Lincoln, Nebraska.

Ping, C. L., J. G. Bockheim, J. M. Kimble, G. J. Michaelson, and D. A. Walker (1998), Characteristics of cryogenic soils along a latitudinal transect in Arctic Alaska, *J. Geophys. Res.*, *103*(D22), 28917-28928, doi:10.1029/98jd02024.

Prins, M. A., and G. J. Weltje (1999), End-member modelling of grain-size distributions of sediment mixtures, in *Pelagic, Hemipelagic and Turbidite Deposition in the Arabian Sea During the Late Quaternary: Unravelling the Signals of Aeolian and Fluvial Sediment Supply*

as Functions of Tectonics, Sea-Level and Climate Change by Means of End-Member Modelling of Siliclastic Grain-Size Distributions, edited by M. A. Prins, pp. 47-68, Geologica Ultraiectina, Utrecht University, Utrecht.

Pye, K. (1987), *Aeolian Dust and Dust Deposits*, 334 pp., Academic Press, London.

Pye, K. (1995), The nature, origin and accumulation of loess, *Quat. Sci. Rev.*, *14*(7-8), 653-667, doi:10.1016/0277-3791(95)00047-X.

Reineck, H. E., and I. B. Singh (1980), *Depositional Sedimentary Environments*, 2nd ed., 549 pp., Springer, Berlin, Heidelberg, New York.

Rigor, I. G., R. L. Colony, and S. Martin (2000), Variations in surface air temperature observations in the Arctic, 1979-97, *J. Climate*, *13*(5), 896-914.

Romanovskii, N. N. (1993), *Fundamentals of Cryogenesis of Lithosphere*, Moscow University Press, 336 pp., Moscow.

Schirrmeister, L., C. Siegert, T. Kuznetsova, S. Kuzmina, A. Andreev, F. Kienast, H. Meyer, and A. Bobrov (2002), Paleoenvironmental and paleoclimatic records from permafrost deposits in the Arctic region of northern Siberia, *Quat. Int.*, *89*, 97-118, doi:10.1016/S1040-6182(01)00083-0.

Schirrmeister, L., D. Froese, V. Tumskoy, G. Grosse, and S. Wetterich (2011a), Yedoma: Late Pleistocene ice-rich syngenetic permafrost of Beringia, in *Encyclopedia of Quaternary Science*, edited by S. A. Elias, Elsevier Science, Amsterdam, accepted.

Schirrmeister, L., G. Grosse, S. Wetterich, P. P. Overduin, J. Strauss, E. A. G. Schuur, and H.-W. Hubberten (2011b), Fossil organic matter characteristics in permafrost deposits of the northeast Siberian Arctic, *J. Geophys. Res., 116*, G00M02, doi:10.1029/2011JG001647.

Schirrmeister, L., V. Kunitsky, G. Grosse, S. Wetterich, H. Meyer, G. Schwamborn, O. Babiy, A. Derevyagin, and C. Siegert (2011c), Sedimentary characteristics and origin of the Late Pleistocene Ice Complex on northeast Siberian Arctic coastal lowlands and islands - A review, *Quat. Int.*, *241,* 3-25, doi:10.1016/j.quaint.2010.04.004.

Schuur, E. A. G., J. Bockheim, J. G. Canadell, E. Euskirchen, C. B. Field, S. V. Goryachkin, S. Hagemann, P. Kuhry, P. M. Lafleur, H. Lee, G. Mazhitova, F. E. Nelson, A. Rinke, V. E. Romanovsky, N. Shiklomanov, C. Tarnocai, S. Venevsky, J. G. Vogel, and S. A. Zimov (2008), Vulnerability of permafrost carbon to climate change: Implications for the global carbon cycle, *BioScience*, *58*(8), 701-714, doi:10.1641/b580807.

Schwamborn, G., A. Förster, B. Diekmann, L. Schirrmeister, and G. Fedorov (2008), Mid- to late-Quaternary cryogenic weathering conditions at Elgygytgyn Crater, northeastern Russia: Inference from mineralogical and microtextural properties of the sediment record, in *9th International Conference on Permafrost*, edited by D. L. Kane and K. M. Hinkel, pp. 1601-1606, Institute of Northern Engineering - University of Alaska Fairbanks, Fairbanks.

Seppälä, M. (2004), *Wind as a Geomorphic Agent in Cold Climates*, 368 pp., Cambridge University Press, Cambridge, United Kingdom.

Sher, A. V. (1971), *Mammals and Stratigraphy of the Pleistocene of the Extreme Northeast of the USSR and North America*, Nauka Publishing, Moscow.

Sher, A. V. (1995), Is there any real evidence for a huge shelf ice sheet in East Siberia?, *Quat. Int.*, *28*, 39-40.

Sher, A. V., T. N. Kaplina, R. E. Giterman, A. V. Lozhkin, A. A. Arkhangelov, S. V. Kiselyov, Y. V. Kouznetsov, E. I. Virina, and V. S. Zazhigin (1979), Late Cenozoic of the Kolyma Lowland, paper presented at 14th Pacific Science Congress, Academy of Science, Khabarovsk, USSR.

Sher, A. V., S. A. Kuzmina, T. V. Kuznetsova, and L. D. Sulerzhitsky (2005), New insights into the Weichselian environment and climate of the East Siberian Arctic, derived from fossil insects, plants, and mammals, *Quat. Sci. Rev.*, *24*(5-6), 533-569, doi:10.1016/j.quascirev.2004.09.007.

Smalley, I. J., and V. Smalley (1983), Loess material and loess deposits: Formation, distribution and consequences, in *Developments in Sedimentology 38 - Eolian Sediments and Processes*, edited by M. E. Brookfield and T. S. Ahlbrandt, pp. 51-68, Elsevier, Amsterdam.

Sun, D., J. Bloemendal, D. K. Rea, J. Vandenberghe, F. Jiang, Z. An, and R. Su (2002), Grain-size distribution function of polymodal sediments in hydraulic and aeolian environments, and numerical partitioning of the sedimentary components, *Sedimentary Geology, 152*(3-4), 263-277, doi: 10.1016/s0037-0738(02)00082-9.

Svendsen, J. I., H. Alexanderson, V. I. Astakhov, I. Demidov, J. A. Dowdeswell, S. Funder, V. Gataullin, M. Henriksen, C. Hjort, M. Houmark-Nielsen, H.-W. Hubberten, O. Ingolfsson, M. Jakobsson, K. H. Kjaer, E. Larsen, H. Lokrantz, J. P. Lunkka, A. Lysa, J. Mangerud, A. Matiouchkov, A. Murray, P. Moller, F. Niessen, O. Nikolskaya, L. Polyak, M. Saarnisto, C. Siegert, M. J. Siegert, R. F. Spielhagen, and R. Stein (2004), Late quaternary ice sheet history of northern Eurasia, *Quat. Sci. Rev.*, *23*(11-13), 1229-1271, doi:10.1016/j.quascirev.2003.12.008.

Tarnocai, C., J. G. Canadell, E. A. G. Schuur, P. Kuhry, G. Mazhitova, and S. Zimov (2009), Soil organic carbon pools in the northern circumpolar permafrost region, *Global Biogeochem. Cycles*, *23*(2), GB2023, doi:10.1029/2008gb003327.

Vasil'chuk, Y. K. (1992), *Oxygen Isotope Composition of Ground Ice - Application to Paleogeocryological Reconstructions*, 420 pp., Geological Faculty of Moscow State University, Moscow.

Vasil'chuk, Y. K., R. A. Vaikmae, J.-M. K. Punning, and M.O. Leibman (1988), Oxygen-isotope distribution, palynology and hydrochemistry wedge ice in organic-mineral complex of Duvanny Yar type section, *Transactions (Doklady) of the USSR Academy of Sciences, Earth Science Section 292*(5), 69-72.

Vasil'chuk, Y. K., A. C. Vasil'chuk, D. Rank, W. Kutschera, and J. C. Kim (2001), Radiocarbon dating of delta O-18-delta D plots in Late Pleistocene ice-wedges of the Duvanny Yar (Lower Kolynia River, Northern Yakutia), *Radiocarbon*, *43*(2B), 541-553.

Velichko, A. A., Y. M. Kononov, and M. A. Faustova (1997), The last glaciation of Earth: Size and volume of ice-sheets, *Quat. Int.*, *41-42*, 43-51.

Walger, E. (1962), Die Korngrößenverteilung von Einzellagen sandiger Sedimente und ihre genetische Bedeutung, *Geol. Rundsch.*, *51*(2), 494-507, doi:10.1007/BF01820015.

Walter, K. M., S. A. Zimov, J. P. Chanton, D. Verbyla, and F. S. Chapin (2006), Methane bubbling from Siberian thaw lakes as a positive feedback to climate warming, *Nature*, *443*(7107), 71-75, doi:10.1038/nature05040.

Welker, J. M., P. A. Wookey, A. N. Parsons, M. C. Press, T. V. Callaghan, and J. A. Lee (1993), Leaf carbon isotope discrimination and vegetative responses of Dryas octopetala to temperature and water manipulations in a high Arctic polar semi-desert, Svalbard, *Oecologia*, *95*(4), 463-469, doi:10.1007/bf00317428.

Weltje, G. J. (1997), End-member modeling of compositional data: Numerical-statistical algorithms for solving the explicit mixing problem, *Math. Geol.*, *29*(4), 503-549, doi:10.1007/bf02775085.

Weltje, G. J., and M. A. Prins (2007), Genetically meaningful decomposition of grain-size distributions, *Sediment. Geol.*, *202*(3), 409-424, doi:10.1016/j.sedgeo.2007.03.007.

Wetterich, S., L. Schirrmeister, A. A. Andreev, M. Pudenz, B. Plessen, H. Meyer, and V. V. Kunitsky (2009), Eemian and Late Glacial/Holocene palaeoenvironmental records from permafrost sequences at the Dmitry Laptev Strait (NE Siberia, Russia), *Paleogeogr. Paleoclimatol. Paleoecol.*, *279*(1-2), 73-95, doi:10.1016/j.palaeo.2009.05.002.

Wetterich, S., L. Schirrmeister, and A. L. Kholodov (2011), *Reports on Polar and Marine Research 636 - The joint Russian-German expedition Beringia/Kolyma 2008 during the*

International Polar Year (IPY) 2007/2008, 43 pp., Alfred-Wegener-Institute for Polar and Marine Research, Bremerhaven.

Wolfe, S. A., A. Gillis, and L. Robertson (2009), Late Quaternary Aeolian Deposits of Northern North America: Age and Extent, *Geological Survey of Canada*, Ottawa.

Wright, J., B. Smith, and B. Whalley (1998), Mechanisms of loess-sized quartz silt production and their relative effectiveness: Laboratory simulations, *Geomorphology*, *23*(1), 15-34.

Zanina, O. G., S. V. Gubin, S. A. Kuzmina, S. V. Maximovich, and D. A. Lopatina (2011), Late-Pleistocene (MIS 3-2) palaeoenvironments as recorded by sediments, palaeosols, and ground-squirrel nests at Duvanny Yar, Kolyma lowland, northeast Siberia, *Quat. Sci. Rev.*, doi:10.1016/j.quascirev.2011.01.021.

Zech, M., R. Zech, W. Zech, B. Glaser, S. Brodowski, and W. Amelung (2008), Characterisation and palaeoclimate of a loess-like permafrost palaeosol sequence in NE Siberia, *Geoderma, 143*(3-4), 281-295, doi: 10.1016/j.geoderma.2007.11.012.

Zimov, S. A., S. P. Davydov, G. M. Zimova, A. I. Davydova, E. A. G. Schuur, K. Dutta, and F. S. Chapin (2006a), Permafrost carbon: Stock and decomposability of a globally significant carbon pool, *Geophys. Res. Lett.*, *33*(20), doi:10.1029/2006gl027484.

Zimov, S. A., E. A. G. Schuur, and F. S. Chapin (2006b), Permafrost and the Global Carbon Budget, *Science*, *312*(5780), 1612-1613, doi:10.1126/science.1128908.

Figure captions

Figure 1: Location of the Duvanny Yar study site and the area of ice-rich permafrost deposit distribution in arctic and subarctic lowlands in the region of late Pleistocene Beringia. From *Schirrmeister et al.* [2011a], based on *Romanovskii* [1993] for Siberian Yedoma Ice Complex deposits, *Péwé* [1975] and *Wolfe et al.* [2009] for North American loess, *Ehlers and*

Gibbard [2003] for last glacial maximum glaciation, and *Brown et al.* [1997] for ground-ice content. Map compiled by G. Grosse (University of Alaska Fairbanks).

Figure 2: Scheme and photo of the composite Yedoma Ice Complex profiles (a) DY-05 and (b) DY-01. The paleocryosol sequence (1.3 to 6.8 m a.r.l.) including the paleocryosols 1 to 3 and paleocryosols 4 and 5 are labeled accordingly. Modified after *Wetterich et al.* [2011]
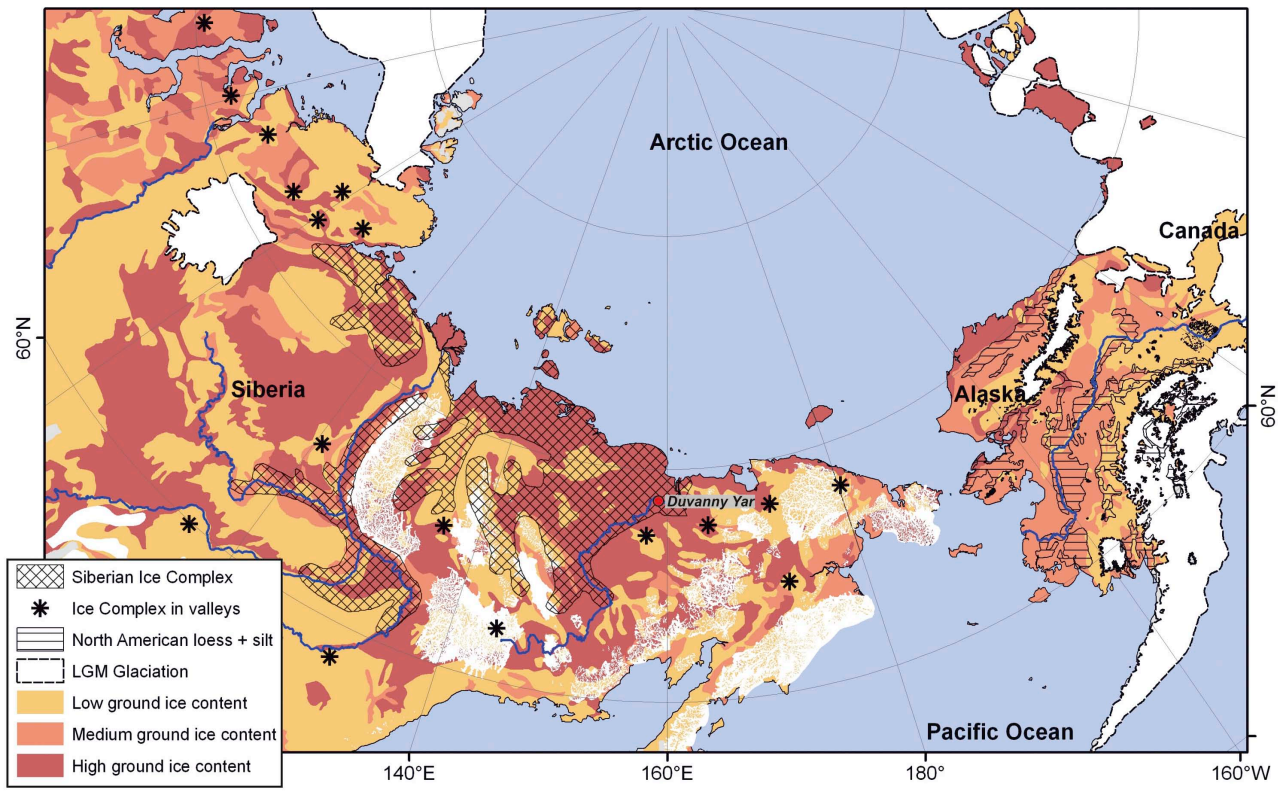
Figure 3: (a) Example of peak fitting for one sample and an explanation of the interactive peak fitter outputs. For comparison the end-member distributions are added; (b) Correlation of peak pairs 3 and 2, and (c) pairs 5 and 4.

Figure 4: Summary of sedimentological and organic-carbon parameters for the Yedoma Ice Complex profiles DY-05 and DY-01. The grain-size fractions are illustrated as follows: clay: light gray, silt: white with black dots, sand: dark gray. The paleocryosols are highlighted with horizontal grey bars labeled from 1 to 5. At the paleocryosol sequence (1.3 to 6.8 m a.r.l) the whole sequence is highlighted. The labeled paleocryosols 1 to 3 are marked with dark grey boxes.

Figure 5: Grain-size distributions of the Yedoma Ice Complex samples as individual representations against profile depth with a view from (a) the side and (b) above. No trend of shifting peak location is obvious in either view.

Figure 6: End-member modeling results. (a) Mean coefficient of determination of all size classes for each end member model. (b) Grain-size distributions of the two end members with natural end member from Alaskan (Vault Creek Tunnel near Fairbanks, Alaska, USA; data from *Schirrmeister*, unpublished) and Chinese (Yulin, northern part of the Loess Plateau, China; data from *Sun et al.* [2002]) loess as well as Chinese floodplain deposits (Bahe formation, Shaanxi Province, northern China; data from *Kenkkilä* [2005]). (c) Coefficients of determination for each sample of the model with two end members. (d) Coefficients of determination for each size class of the model with two end members.

Figure 7: Variation of the end-member and interactive peak fitter scores. Laser-derived grain-size distributions (right) are stacked for sections with similar shape, and variability of each grain-size class within these sections is indicated by error bars. The grain-size fractions are labeled as clay (Cl), silt (Si), and sand (Sa). Background boxes indicate paleocryosols according to **Fig. 4**.

Legend:
- ▨ Siberian Ice Complex
- ✳ Ice Complex in valleys
- ▤ North American loess + silt
- ⬚ LGM Glaciation
- ▨ Low ground ice content
- ▨ Medium ground ice content
- ▨ High ground ice content

Arctic Ocean

Siberia

Alaska

Canada

Duvanny Yar

Pacific Ocean

60°N

140°E   160°E   180°   160°W

Figure caption / panel labels:

(a) E ... W

altitude [m a.r.l.]

Legend:
- [10] sediment samples
- ⅄ larger wood fragments (twigs, roots)
- ⬭ peat inclusion in paleocryosol
- ◿ ice wedges

DY-05-H, DY-05-G, DY-05-F, DY-05-E, DY-05-D, DY-05-C, DY-05-B, DY-05-A

paleocryosol 4, paleocryosol 3, paleocryosol sequence, paleocryosol 2, paleocryosol 1, thermoterrace

(b) DY-01-B, DY-01-C, DY-01-D, DY-01-E, DY-01-F, DY-01-G, DY-01-H, paleocryosol 3

(a) Grain size distribution with estimated model, Gaussian curves, measured grain size, and Gaussian peak numbers across Clay, Silt, and Sand fractions.

(b) area peak 3 vs area peak 2:
$y = -0.99x + 0.55$
$R^2 = 0.85$
$n = 90$

(c) area peak 5 vs area peak 4:
$y = -0.59x + 0.28$
$R^2 = 0.67$
$n = 90$

(a) | Clay | Silt | Sand | grain size [µm] | volume percent [vol%] | DY-01 | DY-05

(b) | Clay | Silt | Sand | altitude [m a.r.l.] | grain size [µm] | volume percent [vol%] | DY-01 | DY-05

End-Member Modeling

alluvial/fluvial/lacustrine processes — aeolian processes

Interactive Peak Fitting

alluvial/fluvial/lacustrine processes — aeolian processes — fluvial/aeolian processes

profile DY-01

profile DY-05

altitude [m a.r.l.]

EM 2 — EM 1 — Peak 5+4 — Peak 3+2 — Peak 1